Journal of Machine Engineering, 2024, Vol. 24
ISSN 1895-7595 (Print) ISSN 2391-8071 (Online)

Received: *02 October 2023* / Accepted: *10 December 2023* / Published online: *28 December 2023*

machine tool, enclosures,
thermal deformation,
FEM thermal analysis

Ikuo TANABE[1*]
Naohiko SUZUKI[2]
Yoshiaki ISHINO[2]
Hiromi ISOBE[3]

DEVELOPMENT OF FEM THERMAL SIMULATION TECHNOLOGY FOR MACHINE TOOL WITH ENCLOSURES AND ITS APPLICATION

These days, most machine tools are interlocked by an enclosure for safety control. At that time, internal heat generation in machine tools first causes thermal deformation of the machine structure, which reduces the machining accuracy of the workpiece. Furthermore, the internal heat generation heats the air inside the enclosure, causing a heat build-up phenomenon, and the trapped heat causes re-thermal deformation of the machine tool structure. As a result, machine tools with enclosures are subject to extremely complex thermal deformation. On the other hand, we would like to use FEM thermal simulation to study thermal deformation countermeasures for machine tools with enclosures at the design stage, but it is difficult to analyse the heat build-up phenomenon using conventional FEM thermal simulation. In this research, the new FEM thermal simulation technology for the heat build-up phenomenon was developed and heat build-up phenomenon in a CNC lathe with enclosure was calculated using the proposed FEM simulation technology. As a result, it had been concluded that the proposed FEM simulation could calculate with high accuracy for the phenomenon of heat build-up in a CNC lathe with enclosure, and the proposed technology is very effective in the design.

1. INTRODUCTION

High-precision industrial products are demanded, which in machine require high-precision machining of machine tools. Thermal countermeasures are essential for high-precision machining [1]. Thermal countermeasures are often used to reduce thermal deformation of machine tools [2–5] and forced cooling [6, 7]. In such cases, FEM (Finite Element Method) thermal simulation is effectively used to qualitatively and quantitatively understand thermal problems of machine tools in advance during the design and development stages, and to study countermeasures against them. In recent years, machine tools must be interlocked for safety, and machine tools with enclosures and TVS (Thermal-Volumetric Space) are common

[1] School of Engineering, Sanjo City University, Japan
[2] Research and Development Section, Takamaz Machinery, Japan
[3] Department of Mechanical Engineering, Nagaoka University of Technology, Japan
E-mail: tanabe@mech.nagaokaut.ac.jp / tanabe.ikuo@sanjo-u.ac.jp
https:doi.org/10.36897/jme/176716

(hereinafter referred to as machine tools with total enclosure). However, this internal heat source of the machine tool transfers heat to the air in the total enclosure, which acts as a new internal heat source to re-thermally deform the machine tool structure, resulting in extremely complex thermal deformation [8–11]. Nowadays, it has become common practice to cover the main body of a machine with a total enclosure, and urgent research on this is desired [12–14] but at present there are no similar research reports in Japan or overseas, although it is urgent and essential.

Therefore, in this research, the new FEM thermal simulation technology for the thermal behaviour in a machine tool with enclosures was developed. Then the thermal behaviour in a CNC lathe with enclosure was experimented for evaluation the proposed FEM simulation technology.

2. NEW FEM THERMAL SIMULATION TECHNOLOGY FOR MACHINE TOOL WITH TOTAL ENCLOSURE

2.1. OUTLINE FOR NEW FEM THERMAL SIMULATION USING TWO VIRTUAL ELEMENTS

Figure 1 shows the two virtual elements to be used by the new FEM thermal simulation. This represents the behaviour of the flowing medium in the structure. It consists of two elements; *I*: Simulated element for boundary layer and *II*: Simulated element for convection. *I* is used for the boundary layer of the total enclosure and is used for the convection of the total enclosure. These two virtual elements are fabricated as solid models using the cavity function during CAD.

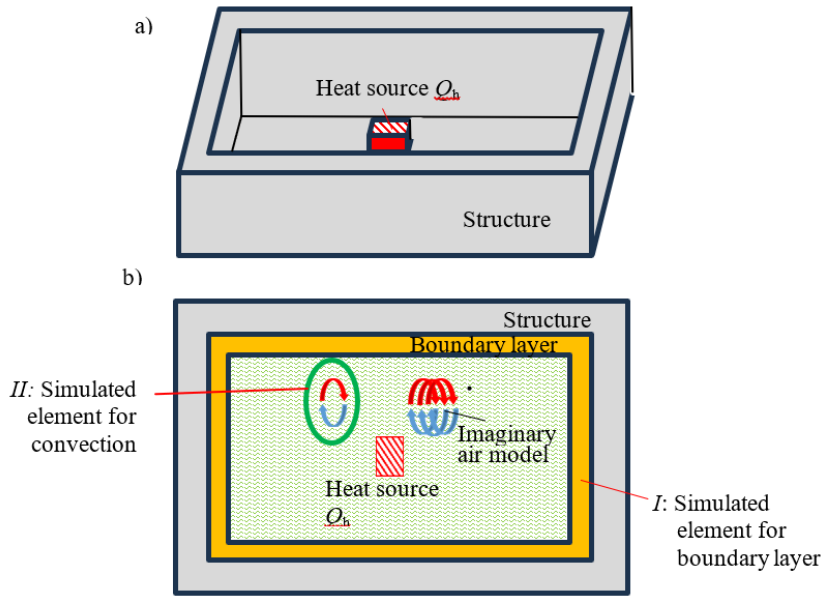

Fig. 1. Two virtual elements *I* and *II* were used for the new FEM: a) Schematic view of a structure with a heat source (Top lid is hidden), b) Schematic view of analysis object for FEM thermal simulation

2.2. EXPLANATION OF THE SIMULATED ELEMENT FOR BOUNDARY LAYER

As shown in Fig. 2, the heat quantity is transferred by heat transfer between the inner wall of the structure and the flowing medium in the structure in Δt [s]. In this case, the amount of heat transferred at the wall surface of the structure by the heat transfer is Q_b [J]. In the case of the Simulated element for boundary layer, the thermal conductivity λ_b [W/mK] is set to simulate the heat transfer for the Q_b [J]. The equivalent states are shown in Equation (1) and (2).

$$Q_b = \alpha_w (T_{b1} - T_{b2}) A_w \Delta t = (\lambda_b / l_b) (T_{b1} - T_{b2}) A_w \Delta t \tag{1}$$

$$\lambda_b = \alpha_w l_b \tag{2}$$

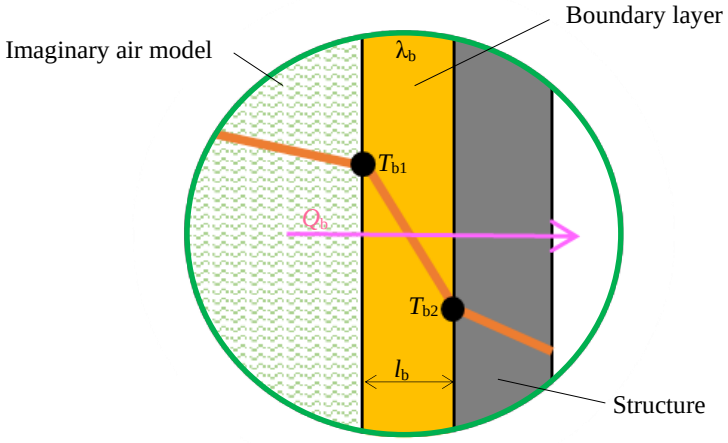

Fig. 2. Explanation of Simulated element for boundary layer (Q_h transfer to the structure during Δt). Heat transfer of the boundary layer was supposed by heat conduction

Where, α_w [W/m^{2}K] is real heat transfer coefficient on the inner wall of the structure, T_{b1} [K] is the temperature of the flowing medium in contact with the Simulated element for boundary layer, T_{b2} [K] is the temperature of the inner wall of the structure in contact with the boundary layer, A_w is surface area of the inner wall of the structure [m^2], λ_b [W/mK] is thermal conductivity for the simulation of the boundary layer and l_b [m] is the thickness of the boundary layer. By inputting the thermal conductivity λ_b to the Simulated element for boundary layer in the enclosure fabricated by the cavity function in CAD, it is possible to simulate the heat transfer phenomena on the structural wall inside the enclosure.

2.3. EXPLANATION OF THE SIMULATED ELEMENT FOR CONVECTION

The energy balance of the flow medium in the structure is considered by replacing it with the elements shown in Fig. 3. Considering the energy balance [15], the following assumptions are made a: The velocity and temperature fields are steady, and the air flow is laminar.

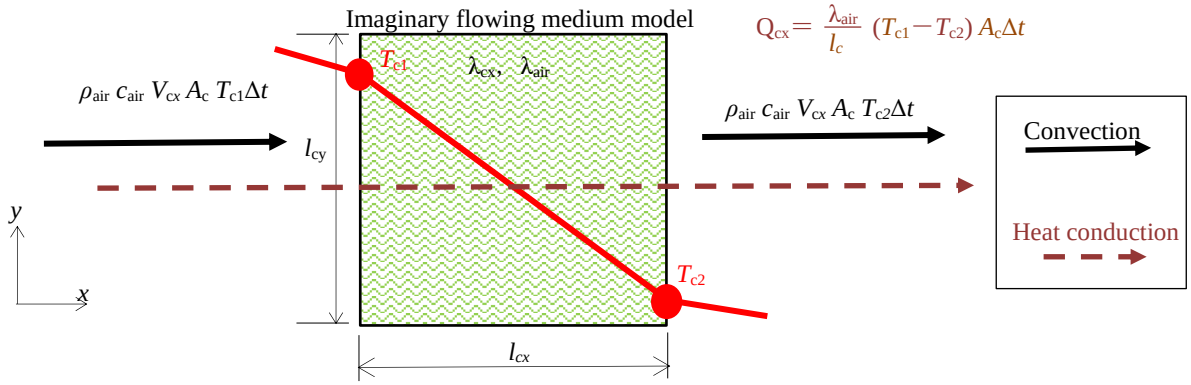

Fig. 3. Energy balance of an element for *x* direction in structure. Convection in the structure was supposed by heat conduction

b:The physical properties (density, viscosity, thermal conductivity and specific heat at constant pressure) are constant. c: Ignoring heat generation in viscous work. As the thermal conductivity of the Simulated element for convection in Fig. 1, the pseudo-thermal conductivity λ_{cx} (heat transfer coefficient that simulates the convection phenomenon) is defined. The heat quantity Q_{cx} [J] moving through the elements in Δt seconds is given by Equation (3). The heat transfer $Q_{cx'}$ [J/s] per unit time due to the heat transfer caused by the temperature difference between the two ends of the elements in Fig. 3 is given by Equation (4). In the x-axis direction, the difference between the energy exerted by convection from the right side of the micro-element and the energy inflowed by convection from the left side of the microelement is given by Equation (5). Since the sum of the heat transferred by heat conduction in Equation (4) and the energy transferred by convection in Equation (5) is the heat of Equation (3), Equation (6) is obtained. To organize this Equation (6), the pseudo-thermal conductivity λ_{cx} is shown in the equation from Equation (7), the pseudo-thermal conductivity of a virtual fluid element to simulate convection can be obtained; we have proposed the pseudo-thermal conductivity λ_{cx} in the x-direction, but the pseudo-thermal conductivities λ_{cy} and λ_{cz} in the y-direction and *z*-direction can also be obtained by the same equation.

$$Q_{cx} = (\lambda_{cx} / l_{cx})\,(T_{c1} - T_{c2})\, A_c \Delta t \tag{3}$$

$$Q_{cx}' = (\lambda_{air} / l_c)\,(T_{c1} - T_{c2})\, A_c \Delta t \tag{4}$$

$$\rho_{air}\, c_{air}\, V_{cx}\, A_c\, T_{c1}\Delta t - \rho_{air}\, c_{air}\, V_{cx}\, A_c\, T_{c2}\Delta t = \rho_{air}\, c_{air}\, V_{cx}\, A_c\, (T_{c1} - T_{c2})\Delta t \tag{5}$$

$$\rho_{air}\, c_{air}\, V_{cx}\, A_c\, (T_{c1} - T_{c2})\Delta t + (\lambda_{air} / l_c)\,(T_{c1} - T_{c2})\, A_c \Delta t = (\lambda_{cx} / l_{cx})\,(T_{c1} - T_{c2})\, A_c \Delta t \tag{6}$$

$$\lambda_{cx} = \lambda_{air} + \rho_{air}\, c_{air}\, V_{cx}\, l_{cx} \tag{7}$$

Where, λ_{cx} [W/mK] is pseudo-thermal conductivity of the element in the x-direction, l_{cx} [m] is length of the element in the x-direction, T_{c1} [K] is temperature of the left end of the element, T_{c2} [K] is temperature of the right end of the element, ρ_{air} [kg/m^3] is density of air, c_{air} [J/kgK] is specific heat of air, A_c [m^2]is the cross-sectional area of the *yz* plane of the element, λ_{air} [W/mK] is pseudo-thermal conductivity of the flow medium in the *x*-direction, V_{cx} [m/s] is the average velocity of air in the *x*-direction. When performing FEM thermal simulations, convection phenomena in a structure can be simulated by first inputting the physical properties of the air into the simulated element for convection in the enclosure fabricated by the cavity function in CAD and then rewriting the thermal conductivity of the air to be this pseudo-thermal conductivity λ_{cx}.

3. EVALUATION OF FEM THERMAL SIMULATION TECHNOLOGY USING CNC LATHE WITH TOTAL ENCLOSURE

3. 1. EXPERIMENTS USING A CNC LATHE WITH TOTAL ENCLOSURE

To evaluate the industrial effectiveness of the FEM thermal simulation technique proposed in Chapter 2, an evaluation experiment was conducted; CNC lathe with a total enclosure was used to some machine cylindrical parts (see Table 2) for 60 minutes with the workpiece automatically changed by a loader.

Table 1. Specification for the used CNC lathe

Items		Property
Chuck size		8 inch
Spindle	Spindle bearing bore	c100 mm
	Spindle speed	Max. 5,000 min^{-1}
Tool post	Shape	12 square turret
	Maximum movement	X:190, Z:420 mm
	Fast feed speed	X:18, Z:24 m/min
Main spindle motor		AC11/7.5 kW, ϕ 100 3,500 min^{-1}
Width × Depth		1,750×1,535 mm
Controller		FANUC 0i-TF Plus

Fig. 4. Photograph of the used CNC lathe

A loader was used for loading and unloading each part. The loading/unloading time is 15 sec. During machining which the machine body temperature and the ambient temperature in the enclosure were measured. Then followed by the machining accuracy of the cylindrical parts. Table 1 shows the specifications of the CNC lathe used in the experiments, and Fig. 4 shows its photograph. It is a small lathe with a floor space of 1,750×1,535 mm, a 7.5 kW spindle motor, and a maximum spindle speed of 3,500 min^{-1}. A chucking cylinder is used to grip the workpiece. Table 2 shows the cutting conditions. Workpiece was carbon steel (S45C in JIS). The right end of a ϕ 65 mm × 30 mm and ϕ 31 mm × 10 mm stepped round bar was turned (ϕ 20 mm × 10 mm, 5 rough cuts and 1 finish cut), and the same process was repeated for 60 minutes with the workpiece automatically changed by a loader.

Table 2. Cutting conditions for the evaluation experiment

Workpiece material		Carbon steel (S45C in JIS)
Workpiece size		See right figure
Rough cutting (5 times)	Spindle speed	2274 min^{-1}
	Feed speed	0.3mm/rev
	Cutting depth	1.0mm
Finish cutting (1 time)	Spindle speed	3500 min^{-1}
	Feed speed	0.1 mm/rev
	Cutting depth	0.5 mm
Cutting fluid		A3(×20 Dilution)
Room temperature		20±1 ℃

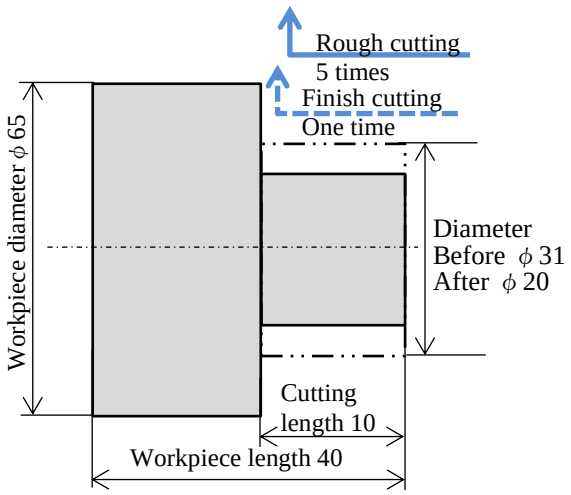

Table 3. Temperature measurement points in the CNC lathe for the evaluation experiment

(a) Structure temperature progression	(b) Structure temperature progression
Coolant tank	Head stock atmosphere
Spindle motor	X-axis slider atmosphere
Spindle rear bearing on cylinder side	Z-axis slider atmosphere
Spindle front bearing on chuck side	Enclosure atmosphere(center)
Chucking cylinder	
X-axis ball screw	
Z-axis ball screw	
Bed	

Wet cutting was performed using a non-water soluble cutting fluid A3 diluted 20 times. Power and hydraulic pressure were turned on 10 minutes before the start of the test. Experiments were conducted in a thermostatic room at 20±1℃. After the turned workpiece was stored in the thermostatic room for at least eight hours, the diameter of only one machined part was measured with a micro-meter because the machining length was only 10 mm. As shown in Table 3, the structural and ambient temperatures at twelve points were measured using T-type thermocouples.

Figure 5 shows the temperature history of the machine tool structure and its atmosphere (experimental results). The temperature progression is indicated by the temperature change from the initial temperature. The temperature change of the coolant tank, spindle motor, and chucking cylinder was large. The temperature rise in the atmosphere around the spindle stand was large. This is due to the internal heat sources of the spindle motor, chucking cylinder, and spindle front/rear bearings, and it is clear that the temperature rise in this atmosphere causes re-thermal deformation of the machine tool structure.

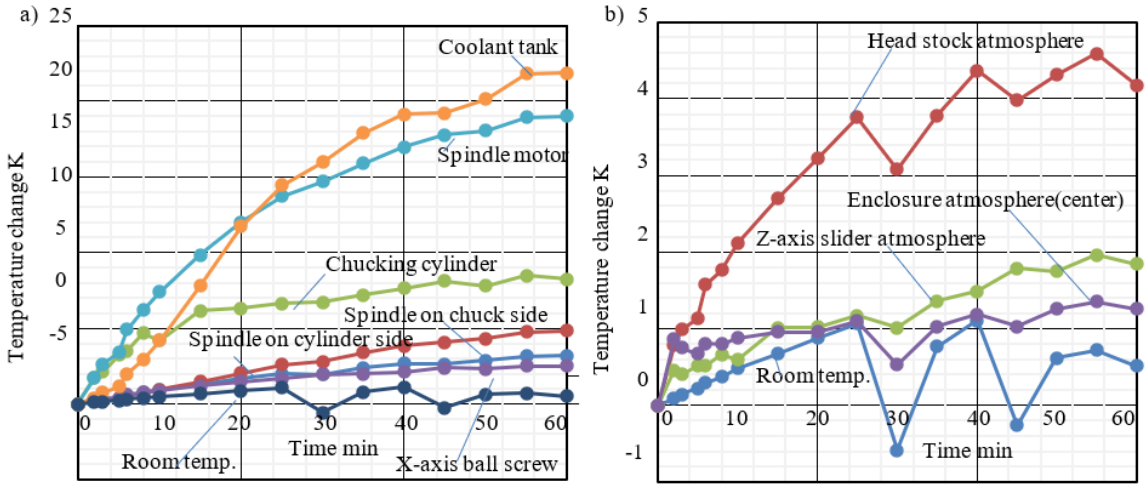

Fig. 5. Experimental results: Temperature changes in the CNC lathe structures and atmosphere: a) Structure temperature progression, b) Atmosphere temperature progression

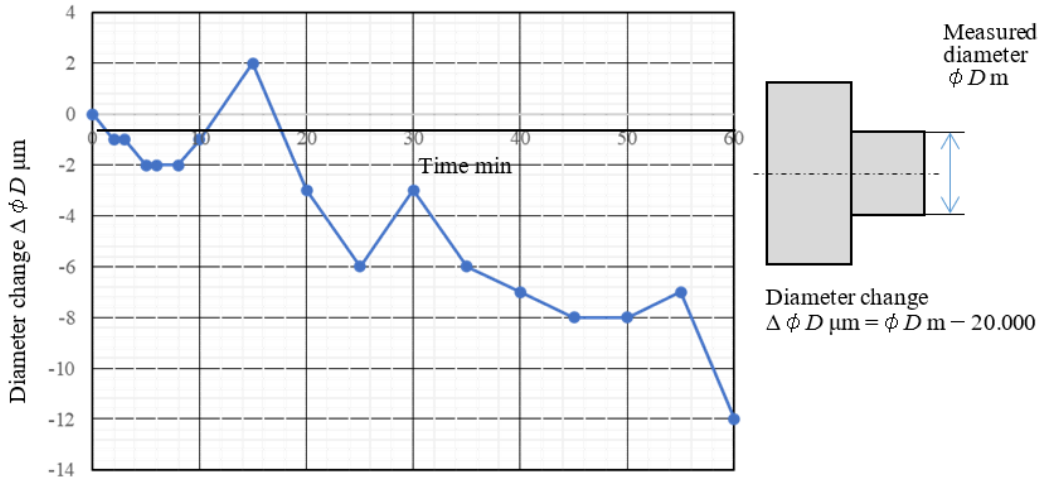

Fig. 6. Experimental result: Accuracy change of the workpiece after finish cutting in the CNC lathe with total enclosure

Figure 6 shows the change in machining accuracy over time (experimental results). The diameter of the finished surface of the workpiece became smaller than ϕ 20 mm over time. This is because the relative distance between the center of the workpiece and the tool tip in the *X*-*Y* plane became shorter due to thermal deformation. These experimental results will be used to evaluate the effectiveness of the FEM thermal simulation technique proposed earlier in the next section.

3.2. ANALYSIS OF CNC LATHE WITH TOTAL ENCLOSURE USING THE PROPOSED FEM THERMAL SIMULATION

Figure 7 and Fig. 8 show a CAD model and an FEM model of a CNC lathe with a total enclosure (see Fig. 4), respectively. The power supply box and control box, which do not directly affect thermal deformation, are omitted here.

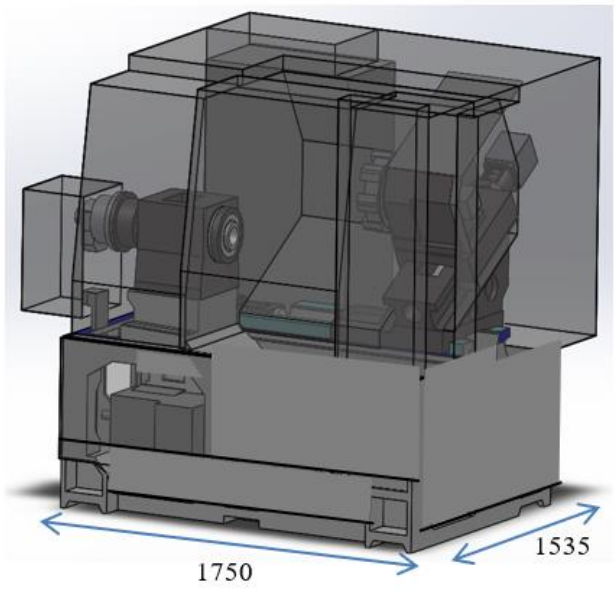

Fig.7. Schematic view of CAD model in CNC lathe with total enclosure

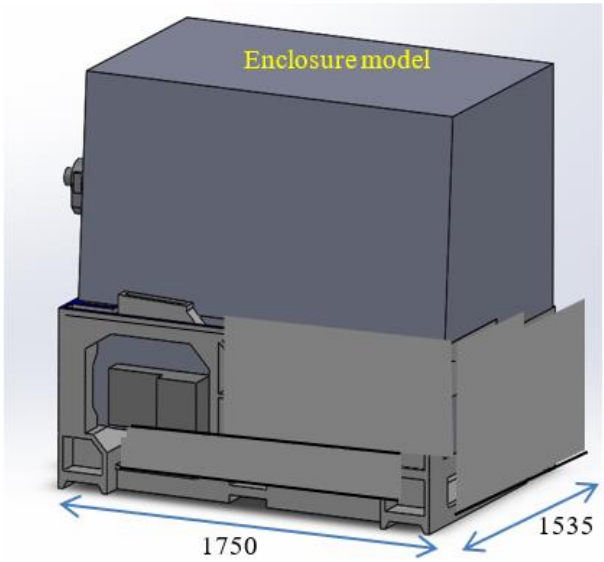

Fig. 8 Schematic view of FEM model in CNC lathe

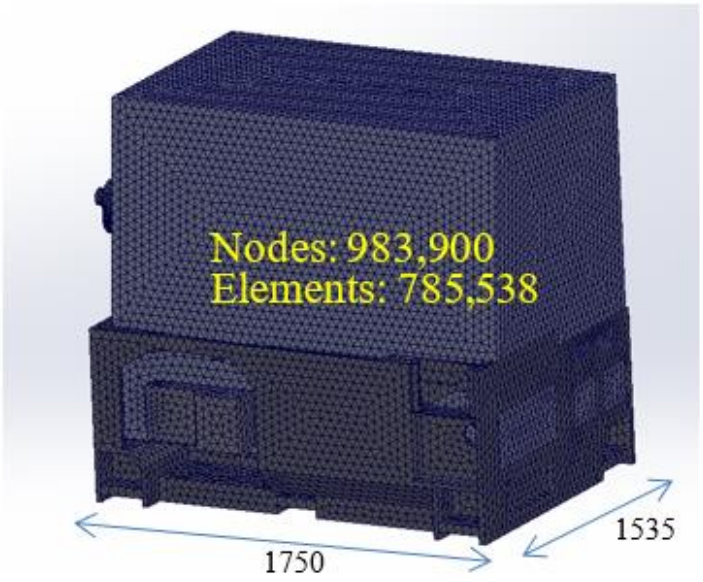

Fig. 9. Schematic view of FEM model with mashing in CNC lathe with total enclosure

Figure 9 shows the FEM mesh model with mesh cutting. Initially, it was difficult to cut the mesh of the FEM model, which consisted of complex shapes and numerous parts. In particular, the FEM model of the total enclosure is a large model with complex and minute parts, and its meshing was extremely difficult. In order to easily mesh-cut the FEM model of a machine tool with a total enclosure, the FEM mesh model shown in Fig. 9 was created by simplifying the mesh model and setting the mesh parameters in SolidWorks' existing functions. Using this model, a FEM thermal analysis was used to calculate the temperature change, followed by a coupled FEM static analysis to calculate the thermal deformation.

Table 4 shows the analysis conditions for the FEM thermal simulations. The thermal conductivity λb for the *I*: Simulated element for boundary layer in the enclosure fabricated by the cavity function in CAD was used 6 W/mK (= α_w:600W/m^{2}K× l_b:0.010m). The pseudo-thermal conductivity λ_{cx} for the *II*: Simulated element for convection in the enclosure fabricated by the cavity function in CAD was used 2462 W/mK (= λ_{air}:0.023 W/mK+ ρ_{air}: 1.1 kg/m^3× c_{air}: 1000J/kgK ×V_{cx}:5m/s × l_{cx}0.5m). In the FEM static analysis, the Young's modulus of the air in the enclosure was reduced to 0.1 GPa so that it would not affect the deformation calculations. In addition, the bottom of the machine was fully fixed (this was also confirmed not to affect the deformation calculations). Figure 10 shows the calculation method for machining accuracy; the workpiece diameter after thermal deformation was calculated from the relative displacement of the workpiece center and tool tip in the *X*-*Y* plane using the results of the FEM static analysis.

Table 4. Analysis conditions for the proposed FEM thermal simulation

Enclosure property	Simulated thermal conductivity for *I*	6 W/mK
	Simulated thermal conductivity for *II*	2462 W/mK
	Simulated Young's modulus	0.1 GPa
	Density	1.1 kg/m^3
	Specific heat	1.0 kJ/kgK
	Linear expansion	1.2×10^{-5} 1/K
Internal heat source	Spindle motor	800 W
	Chucking cylinder	200 W
	Spindle front bearing	200 W
	Spindle rear bearing	40 W
	X-axis ball screw	2.2 W
	Z-axis ball screw	2.2 W
	Coolant tank	22°C, Primary delay
Heat transfer to the outside temperature 0°C		Heat transfer coefficient 15W/m^2 K
Initial temperature of machine structure is 0°C		

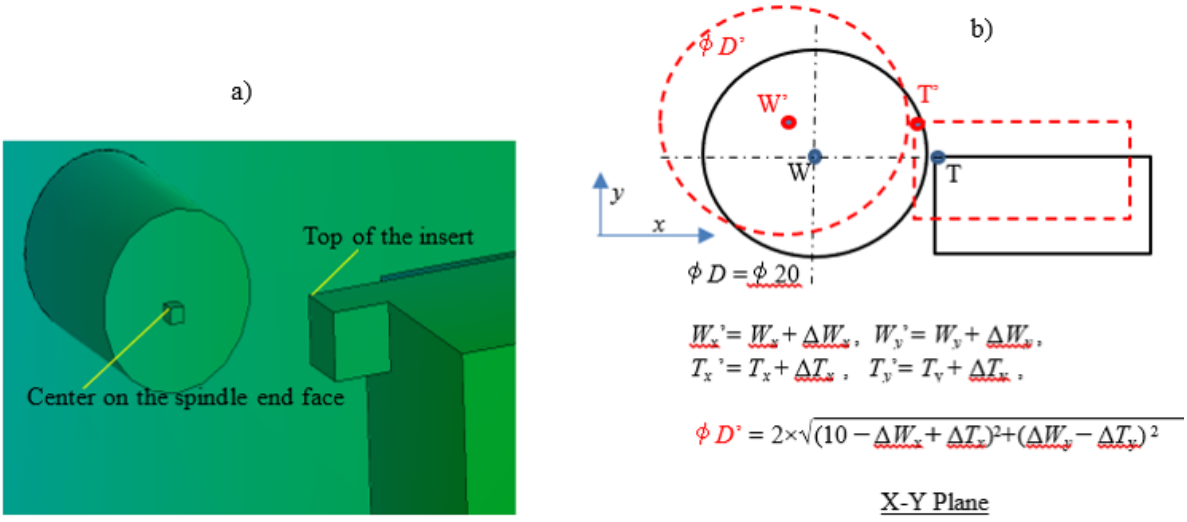

Fig. 10. Calculation method for the accuracy (diameter change) using the analysis results of FEM static simulation: a) Schematic view of thermal deformation, b) Schematic view of thermal deformation

Figure 11 shows an example of the calculated temperature distribution. The ambient temperature (air) in the vicinity of the point where the heat generation rate was set increased, confirming that the FEM thermal simulation technique proposed earlier worked qualitatively to calculate the behaviour of the air inside the enclosure.

Figure 12 shows the temperature progression of the machine tool structure and its atmosphere (analysis results). The results correspond well to the experimental results shown in Fig. 6, confirming that the previously proposed FEM thermal simulation technique works qualitatively and quantitatively to calculate the behaviour (temperature rise) of the air inside the enclosure.

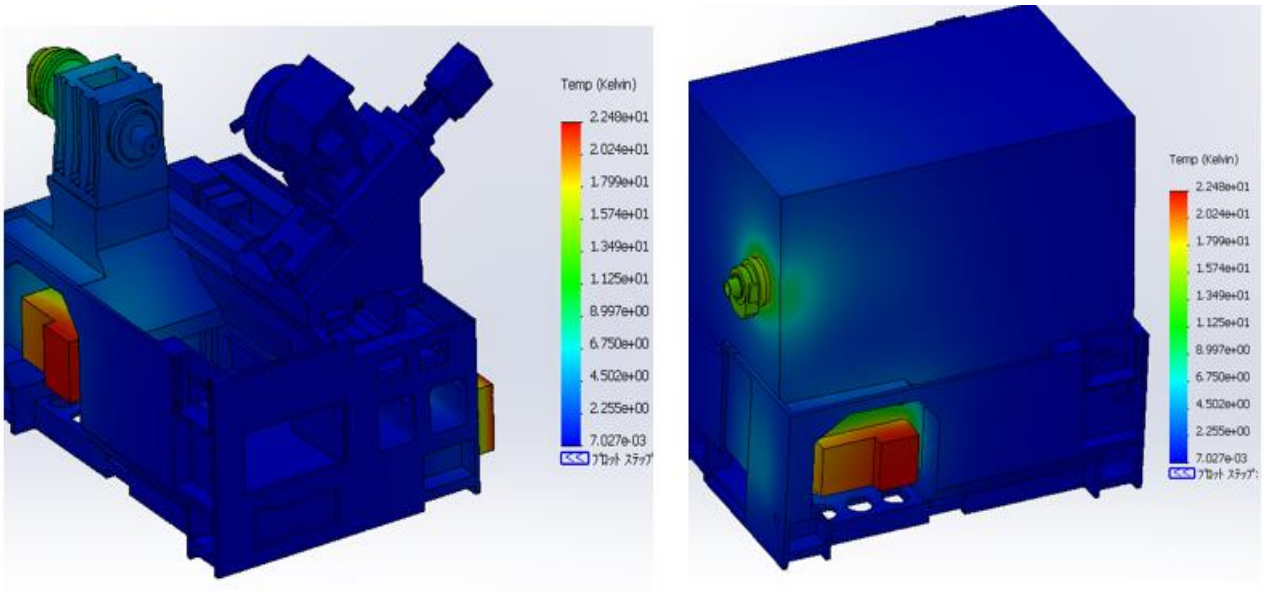

Fig. 11. An example of analysis results: Temperature distribution of the CNC lathe with total enclosure after one hour: a) Enclosure hidden, b) Enclosure display

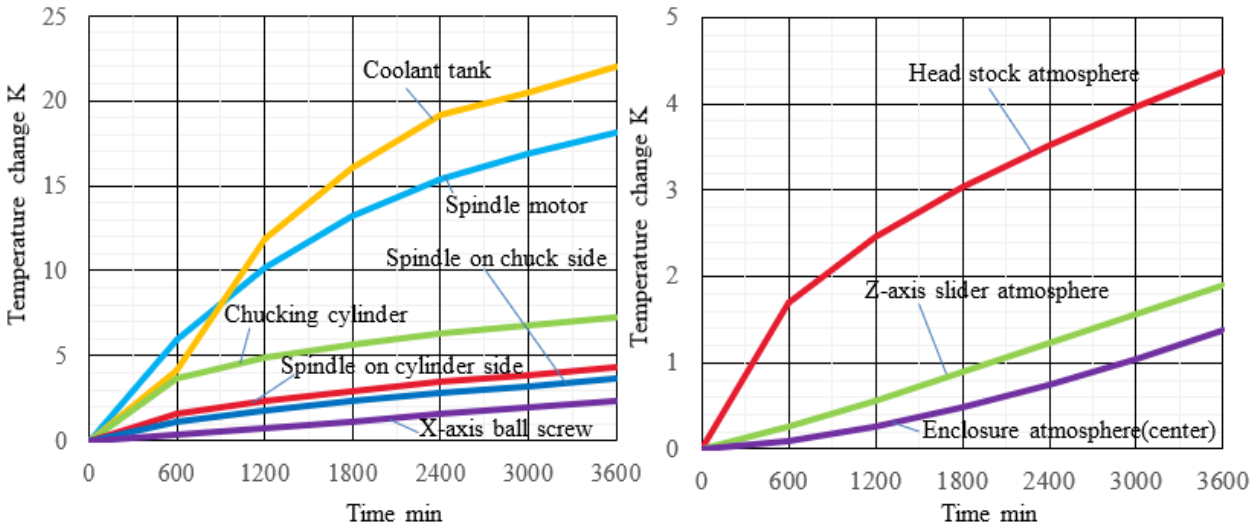

Fig. 12. Analysis results: Temperature changes in the CNC lathe structures and atmosphere: a) Structure temperature progression, b) Atmosphere temperature progression

Figure 13 shows the change over time in machining accuracy (analysis results). The experimental results shown in Fig. 6 are also included for reference. The analysis results correspond well to the experimental results, confirming that the previously proposed FEM thermal simulation technique works qualitatively and quantitatively to calculate the thermal behaviour (thermal deformation and machining accuracy) of a machine tool with a total enclosure.

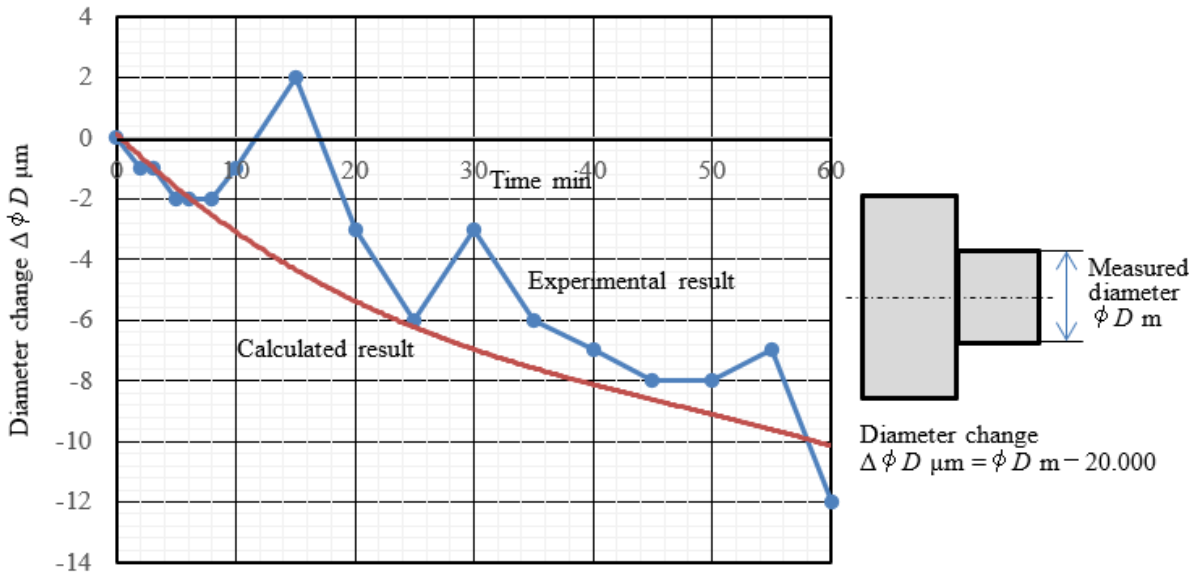

Fig. 13. Analysis and experimental results: Accuracy change of the workpiece after finish cutting in the CNC lathe with total enclosure

As above, the proposed new FEM thermal simulation technique was evaluated to be effective for the calculation of the extremely complex thermal deformation in actual machine tool structure with the total enclosure. Therefore, we believe that the technique will be an effective design tool for future high-precision CNC machine tools.

4. CONCLUSION

To evaluate the industrial effectiveness of the developed FEM thermal simulation technique, a CNC lathe with a total enclosure was used to compare and evaluate the analytical and experimental results of temperature progress and machining accuracy, respectively. The results are summarized as follows; (1) The proposed FEM thermal simulation technique (thermal analysis) was able to calculate the temperature change of the mechanical structure and atmosphere with respect to the heat buildup phenomenon in the enclosure, (2) The proposed FEM thermal simulation technique (static analysis) was able to accurately calculate thermal deformation and processing accuracy with respect to the heat buildup phenomenon in the enclosure, (3) We have proposed a tool to study thermal deformation countermeasures for machine tools with total enclosures.

REFERENCES

[1] GRZESIK W., 2020, *Modelling of Heat Generation and Transfer in Metal Cutting*, Journal of Machine Engineering, 20/1, 24–33, https://doi.org/10.36897/jme/117814.

[2] BRECHER C., HIRSCH P., WECK M., 2004, *Compensation of Thermo-Elastic Machine Tool Deformation Based on Control Internal Data*, CIRP Annals – Manufacturing Technology, 53/1, 299–304.

[3] MARES M., HOREJS O., HORNYCH J., KOHUT P., 2011, *Compensation of Machine Tool Angular Thermal Errors Using Controlled Internal Heat Sources*, Journal of Machine Engineering, 11/4, 78–90.

[4] LANG S., ZIMMERMANN N., MAYR J., WEGENER K., BAMBACH M., 2023, *Thermal Error Compensation Models Utilizing the Power Consumption of Machine Tools*, S. Ihlenfeldt (Ed.): ICTIMT 2023, Springer, LNPE, 41–53, https://doi.org/10.1007/978-3-031-34486-2_4.

[5] MAYR J., JEDRZEJEWSKI J., UHLMANN E., DONMEZ M. A., KNAPP W., Härtig F., WENDT K., MORIWAKI T., SHORE P., SCHMITT R., BRECHER C., WURZ T., WEGENER K., 2012, *Thermal Issues in Machine Tools*, CIRP Annals – Manufacturing Technology, 61, 771–791.

[6] JEDRZEJEWSKI J., WINIARSKI Z., KWASNY W., 2020, *Research on Forced Cooling of Machine Tools and its Operational Effects*, Journal of Machine Engineering, 20/2, 18–38, https://doi.org/10.36897/jme/122769.

[7] MARES M., HOREJS O., FIALA S., HAVLIK L., STRITESKY P., 2020, *Effects of Cooling Systems on the Thermal Behaviour of Machine Tools and Thermal Error Models*, Journal of Machine Engineering, 20/4, 5–27, https://doi.org/10.36897/jme/128144.

[8] JEDRZEJEWSKI J., MODRZYCKI W., 2007, *Compensation of Thermal Displacement of High-speed Precision Machine Tools*, Journal of Mechanical Engineering, 7/1, 108–114.

[9] NGOC H.V., MAYER J.R.R., BITAR-NUHME E., 2023, *Deep Learning to Directly Predict Compensation Values of Thermally Induced Volumetric Errors*, Machines, 11, 496. https://doi.org/10.3390/machines11040496.

[10] TECHNISCHE UNIVERSITAT DRESDEN, 2016, *A Systemic Approach to Solve the Conflict Between Power Efficiency, Accuracy and Productivity Demonstrated at the Example of Machining Production*, Retrieved December 6, 2023 from https://transregio96.webspace.tu-dresden.de/index.php/thermo-energetic-design-of-machine-tools/.

[11] GROSSMANN K., 2016, *Thermo-energetic Design of Machine Tools: A Systemic Approach to Solve the Conflict Between Power Efficiency, Accuracy and Productivity Demonstrated at the Example of Machining Production (Lecture Notes in Production Engineering)*, Springer; Softcover reprint of the original 1st ed., ISBN-10: 3319365460, ISBN-13: 978-3319365466, 1–272.

[12] MAYR J., JEDRZEJEWSKI J, UHLMANN E., et al., 2012, *Thermal Issues in Machine Tools*, CIRP Annals, 61/2, 771–791.

[13] ETA ZURICH, 2012, *Thermal Issues in Machine Tools - Research Collection (ethz.ch)*, Retrieved December 6, 2023 from https://www.research-collection.ethz.ch/handle/20.500.11850/59227.

[14] ITO Y., (2021), *The Untold Story of Machine Tools (Part II: Technology and Skill to Create Models Suitable for Machining Requirements – Importance of Know-How and "Instinct and Inspiration" Capturing the "Essence of Technology" in "Design and Manufacturing Technology" – 4)*, Machines and Tools, October 2021 issue, 116–126, (in Japanese).

[15] SUGIYAMA H., SANO M., NAGAHASI Y., KATO N., 2014, *Transfer Phenomenology to Learn for the First time – to Understand Momentum, Heat, Mass Transfer Integrated –*, Morikita Publication, 110–155 (in Japanese).